Environmental Science and Pollution Research
https://doi.org/10.1007/s11356-024-34698-5

ADVANCED FUNCTIONAL MATERIALS AND DEVICES

KOH-treated tire pyrolyzed carbon as green and easily available adsorbent for Bisphenol A and Methylene blue adsorption

Shiva Deepti Rangu[1,3] · Harsha S. Rangappa[2] · Phyu Phyu Mon[1] · Phyu Phyu Cho[1] · Umamaheswara Rao Mudadla[1] · Subrahmanyam Challapalli[1]

Received: 24 April 2024 / Accepted: 7 August 2024

Abstract

The occurrence of micropollutants and dyes in water sources has sparked alarm due to their significant impacts on aquatic ecosystems and human health. This study aims to utilize the tire pyrolyzed carbon (TPC) as a source of the adsorbent for removing Bisphenol A (BPA) and Methylene Blue (MB). The adsorbent was synthesized by chemical activation of TPC with KOH at 750 °C. The activated TPC was characterized for different physical and chemical characterization techniques such as XRD, FTIR, SEM, BET, XPS, and TPD and exhibits a higher adsorption capacity of 49.2 and 72.1 mg/g respectively for BPA and MB. The effect of initial concentration, dosage of adsorbent, and initial pH are evaluated for BPA and MB. The adsorption is mainly driven by hydrophobic, electrostatic, π-π interactions, and hydrogen bonding. The removal process follows the second order and Langmuir isotherms. The adsorbent shows excellent recyclability which makes it a potential source of removal of different water-borne pollutants. The production of activated carbon from tire waste is advocated for its economic and environmental benefits.

Keywords Tire waste carbon · Bisphenol-A · Methylene Blue · Wastewater treatment · KOH

Introduction

Emerging contaminants (EC) have been widely reported in wastewater in recent times (Naidu et al. 2016). Endocrine disruptive chemicals (EDCs) are regarded as EC which are widely used in anthropogenic activity (Kumar et al. 2022). Bisphenol A (BPA) is one of the most used EDCs. It is abundant in polycarbonate polymers (Abrams and Kremer 2003) and epoxy resins (Ferdosian 2015). Due to the diversified applications, they are in high demand. As a result, BPA production has reached thousands of tons per annum. The BPA can mimic the endocrine hormone leading to negative effects on human health and animals. It also reported that BPA can cause cancerous tumors (Erkekoglu and Koçer-Gümüşel 2017; Hafezi and Abdel-Rahman 2019), may lead to cardiovascular diseases (Chen et al. 2023) and birth defects, and mental disorders even at very low concentrations(Vandenberg et al. 2007; Chen et al. 2023). BPA exposure in the environment at a dose of 10^{-8} M can encourage the migration of cancer cells (Jia et al. 2019). For marine creatures, the presence of BPA in concentrations between 1000 and 10,000 µg/L can be extremely hazardous (Careghini et al. 2015). So, there is an acute need for the remediation of BPA in water and wastewater.

On the other hand, the use of dyes is growing due to the rapid industrial development to meet the demands of population expansion. Industries producing textiles, paper, wool, rubber, plastics, cosmetics, and medicines use cationic dyes (Mehrizad and Gharbani 2016). Cationic dyes are more poisonous than other type of dyes as they are capable of penetrating cell membrane (Sokolov et al. 2023). MB is one of those cationic dyes. It is carcinogenic and mutagenic, and it can even enter the path of photosynthesis, which can lead to

Responsible Editor: Tito Roberto Cadaval Jr

✉ Subrahmanyam Challapalli
csubbu@iith.ac.in

[1] Department of Chemistry, Indian Institute of Technology Hyderabad, Kandi, Sangareddy, Telangana 502285, India

[2] Center for Interdisciplinary Programs, Indian Institute of Technology Hyderabad, Kandi, Sangareddy 502285, Telangana, India

[3] Department of Chemistry, Tara Govt. Degree College(A), Sangareddy 502001, Telangana, India

Published online: 20 August 2024

its entry into to food chain (Ali et al. 2019), causing adverse effects on human health (Gharbani et al. 2022).

There are numerous methods, including adsorption, photocatalysis, Fenton's process, electric coagulation, and biodegradation for wastewater treatment. Nevertheless, these methods do have several drawbacks, including insufficient removal, the formation of sludge, and high running costs (Tabatabaei et al. 2011; Mehrizad and Gharbani 2016; Tursi et al. 2018). Adsorption is a popular water treatment technology for removing waterborne pollutants (Mehrizad et al. 2012) due to its removal efficiency, ease of use, affordability (Mehrizad and Gharbani 2014), high rate of reusability, and minimal production of hazardous sludge. Adsorbents with high carbon contents are typically versatile and can be used effectively to remove both organic and inorganic contaminants (Gupta et al. 2009). These carbonaceous adsorbents have extensive surface area and well distribution of pore sizes (Mehrizad and Gharbani 2014). The activated carbon (AC) was chosen even though alternative materials such as metal–organic frameworks, magnetic nanocomposites, and graphitic material were there, as those materials require more cost, time, and laborious work. However, commercially available AC is expensive (San Miguel et al. 2001), leading to the use of alternative materials such as biowaste (Dural et al. 2011; Tokula et al. 2023), industrial waste (Ali et al. 2012; Soliman and Moustafa 2020), and other substances which can cause damage to the environment if they are not properly addressed.

One viable possibility is discarded tires, which pose a significant disposal challenge. Many of these scrap tires are being used for high-performance road bases and playground covers. These waste tires possess a high calorific value due to their elevated carbon-to-hydrogen ratio. Superior methods are those that conserve energy. Incineration and combustion may come under this, but they are unfit according to risk–benefit analysis as they can cause more damage to the environment (Machin et al. 2017). Numerous investigations and summarization of tire pyrolysis show that pyrolysis is an environment-friendly way to manage waste tires in a profitable way (Zerin et al. 2023). Tire pyrolyzed carbon is a promising source of activated carbon, which minimizes the production cost of activated carbon and reduces the landfill waste (Zerin et al. 2023).

Even though there are attempts to get AC from tire pyrolysis carbon for the removal of several pollutants such as remozal dye (Nogueira et al. 2019), atrazine and ibuprofen (Frikha et al. 2022), BPA (Acosta et al. 2018; Kuśmierek et al. 2020), and for heavy metals (Shahrokhi-Shahraki et al. 2021; Frikha et al. 2022), there is a lag in the study of the capability of the adsorbent of a single treatment in removing a wider range of pollutants.

This study aims to investigate the use of waste rubber tire carbon as an adsorbent with a high carbon content that could have significant adsorption capacity for waterborne pollutants. Activating the tire carbon was done using a chemical method by activating the tire pyrolyzed carbon with KOH at 750 °C for 5 h. Adsorbing model pollutants BPA, a neutral hydrophobic molecule, and MB, a cationic hydrophilic molecule, are used for evaluating the adsorbent. The different factors that affect adsorption, such as contact time, initial pollutant concentration, adsorbent dose, temperature, pH, presence of an electrolyte, and regeneration studies, are examined in a series of experiments to determine the adsorption efficiencies for BPA and MB. Utilizing the equilibrium data obtained to explore kinetics, thermodynamics, and adsorption isotherms.

Experimental

Materials

Tire pyrolyzed carbon used for this study was purchased from India MART, and it is 99%. Potassium hydroxide (KOH) (85%) of SD Fine Chem limited, Sodium chloride (NaCl) (99.9%) (SRL), Sodium hydroxide (NaOH) (85%) (SRL), Bisphenol A (BPA with empirical formula $C_{16}H_{18}O_2$) (97%) (Sigma-Aldrich), Methylene blue (MB with empirical formula $C_{16}H_{18}ClN_3S.3H_2O$), Nitric acid (HNO_3) (65%) (Avra), Hydrochloric acid (HCl) (32%) (Avra), ethanol (C_2H_5OH) (99%) (Sigma-Aldrich), and Sodium nitrite ($NaNO_3$) (99%) (Avra) were purchased from distributors and Millipore water was used for all the experiments. All chemicals were analytical grade and used without further purification.

Preparation of adsorbents

The initial treatment was utilizing varying molar concentrations of KOH (1 M, 2 M, 4 M, 6 M, and 8 M) in 50 mL volumes. A total of 10 g of TPC was sieved to obtain particles with a size ranging from 150 to 75 µm. These particles were then combined with a solution of KOH and well-mixed using a magnetic stirrer at 300 rpm. The mixture was heated until the entire water evaporated, and a dried powder was crushed again. The dried powder was thermally treated in a tubular furnace in the nitrogen atmosphere furnace at a temperature of 750 °C for 5 h. Subsequently, the resulting carbon materials are designated as K-TPAC-1, K-TPAC-2, K-TPAC-4, K-TPAC-6, and K-TPAC-8 (Fig. 1).

Characterization techniques

The X-ray diffraction (XRD) technique was used to investigate the phase purity and transformation of activated carbon produced from pyrolyzed tires. The diffraction patterns were

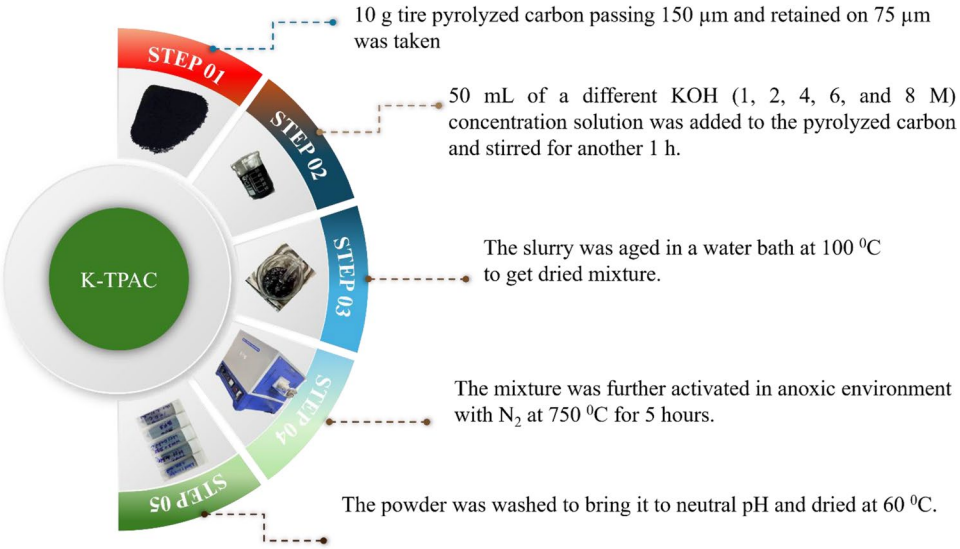

Fig. 1 Preparation of activated carbon from TPC with KOH treatment

recorded using Cu Kα radiation (wavelength of 1.5418 Å). A Ni filter was employed to limit the range of 2θ to 5–80°. The step size for scanning was 0.0167°, and the scan rate was 0.0301°/s. The analyses were performed using the MalvernPANalytical, Empyrean (Netherland) equipment. Scanning electron microscopy (SEM) was done to obtain high-resolution images and sample surface information. The instrument used to take the SEM images is the ZEISS, Sigma 360 VP (Germany). Surface area measurements were conducted using a Quanta chrome, Nova 2200e (USA) surface area analyzer, employing the BET (Brunauer, Emmett, and Teller) method. Before the studies, the samples were subjected to degassing at a temperature of 573 K for 3 h to remove any contaminants present on the sample surface. The temperature-programmed desorption of CO_2 and CO was carried out with the assistance of a chemisorption system (Microtrac BEL Corporation, BELCAT II (Japan)) equipped with a TCD detector. Experiments with He-TPD were conducted to investigate the amount and type of oxygen groups on the adsorbent surface. For this analysis, samples were carried out at a linear heating rate of 10 K/min with a targeted temperature of 1173 K and a constant helium flow of 30 mL/min. The quantification of the CO and CO_2 gases evolved was done by analyzing the signal and the type of oxygen group is predicted based on the temperature at which the gas is evolving. Fourier-transform infrared spectroscopy was used to understand the phase transformation and the functional groups of prepared adsorbents with JASCO, FT/IR 4600 (Japan). X-ray photoelectron spectroscopy (XPS) of prepared adsorbents was done using an Al-K source at 1489.5 eV, emission current, and voltage of 10 mA and 15 kV, respectively. The instrument SCHIMADZU, Axis Supra (Japan), was used for these XPS studies. To test the pHPZC, sodium nitrate solutions (0.1 M) were made with varied initial pH values: 2 to 12 of 25 mL each. To prepare these solutions, the pH is adjusted with 0.05 M aqueous solution of HNO_3 or NaOH. For these solutions, 25 mg of adsorbent was added. Those containers are sealed and kept in an orbital shaker for 24 h and then measured for final pH. The plot of initial pH versus change in pH was drawn. Systronics µ pHSystem 36 l (India) digital pH meter is used to measure the pH of the solution. The T90 + UV–Vis spectrometer MB, manufactured by PG Instruments Ltd. in India, was utilized for the quantification of BPA and pollutants.

Adsorption studies

The initial batch studies were conducted using K-TPAC-1, K-TPAC-2, K-TPAC-4, K-TPAC-6, and K-TPAC-8 for BPA adsorption by taking 50 mL of ppm BPA solution and adsorbent dosage 50 mg, to know the best adsorbent among them. Further experiments were continued with K-TPAC-6 adsorbent for BPA and MB adsorption. The influence of initial pollutant concentrations is measured by taking BPA with initial concentrations of 5, 20, 50, and 75 ppm, while MB concentrations were 20, 50, 100, and 200 ppm. The effect of the adsorbent dose was tested at 0.5, 1, and 1.5 g/L. The impact of pH on BPA and MB adsorption is examined in the pH range of 2 to 10. The effect of ions presence on the adsorption of BPA and MB is examined with 0, 1, 5, 10 mM NaCl present in the pollutant solution. The effects of temperatures 298 K, 308 K, 318 K, and 328 K were investigated for MB and BPA adsorption.

The initial concentration of pollutant used is 20 ppm, and the volume taken is 50 mL. The adsorbent dosage used was 1 g/L, and the agitation speed was set at 200 rpm. The adsorption experiments are conducted at room temperature and the agitation speed is set at 200 rpm. Then, the samples collected were analyzed for BPA & MB concentrations with UV–visible spectrophotometers at wavelengths of 276

and 663 nm, respectively. The adsorption efficiency (%) and adsorption capacity q_t (mg/g) are calculated with the following formulae (1) and (2).

$$\text{Adsorption efficiency}(\%) = \frac{C_0 - C_t}{C_0} X100 \quad (1)$$

$$\text{Adsorption capacity}\left(q_t\right) = \frac{(C_0 - C_t)V}{m} \quad (2)$$

where C_o and C_t are the initial and final concentrations of pollutant in ppm, V is the volume of solution in mL, and m is the mass of adsorbent in g. All the experiments are done thrice and meen of values are considered.

Desorption tests were conducted to assess the potential for reuse, regeneration, and interaction between the adsorbate and the adsorbent. For these studies, 0.5 g of adsorbent was initially mixed with 20 ppm 500 mL of pollutant solution and agitated till the equilibrium was reached. The adsorbent was collected by centrifugation. The spent adsorbent is regenerated with ethanol for BPA and with 0.5 M HCl for MB. The spent adsorbent is treated with respective eluting solution for 15 min followed by centrifuging to separate the solvent, which is analyzed for pollutant concentration. This process continued till the maximum amount of pollutant was removed. Then the adsorbent is dried in an oven at 110 °C and is used for the next cycle.

The desorption efficiency (d) of the solvent and regeneration efficiency or reuse capability (r) of the adsorbent can be measured by following Eqs. (10 and11) (Mpatani et al. 2020):

$$\text{Desorption efficiency}(d) = \frac{\text{quantity of pollutant desorbed}}{\text{total quanity of pollutant on spent adsorbent before desorption}} \text{X } 100 \quad (3)$$

$$\text{Regeneration efficiency}(r) = \frac{\text{adsorption capacity in n}^{\text{th}}\text{ cycle }(q_n)}{\text{adsorption capacity in 1}^{\text{st}}\text{ cycle}(q_1)} X100 \quad (4)$$

Results and discussion

Characterization of adsorbent

The X-ray diffraction plots of TPC and all activated tire pyrolyzed carbons K-TPAC 1–6 can be seen in Fig. 2a. The broad peaks at 2θ values of 25.4 and 47.6 are due to the response of carbon (0 0 2), (1 0 1) planes. These peaks are more pronounced in activated carbons, which show a more amorphous nature of carbon in the respective adsorbents (Dandekar et al. 1998). There are several small sharp peaks at 2θ values of 28.6, 30.6, and 33.2 are the peaks belonging to (1 0 2), (1 0 3), and (1 0 4) planes of ZnS (JCPDS#892739) along with amorphous carbon peak. The peaks at 2θ values of 31.7, 34.3, and 36.2 are because of (1 0 0), (0 0 2), and (1 0 1) planes of ZnO (JCPDS#891397). The peak at 2θ value of 20.2 is because of (0 4 1) plane is SiO_2 (JCPDS#891813).

The strong and broad FTIR peak in the region of 3550 to 3200 cm^{-1} is due to intermolecular hydrogen-bonded -O–H stretching, the peak at 1720 cm^{-1} is C = O stretching carboxylic acid, the medium peak at 1640 cm^{-1} is conjugated C = C stretching, 1543 cm^{-1} is cyclic alkene C = C stretching, 1380 cm^{-1} is O–H or C-H bending vibrations, and the strong and broad peak at 1037 cm^{-1} is anhydride (O = C–O–C = O)functional group (Zhang et al. 2017; Mopoung and Dejang 2021) (Fig. 2b).

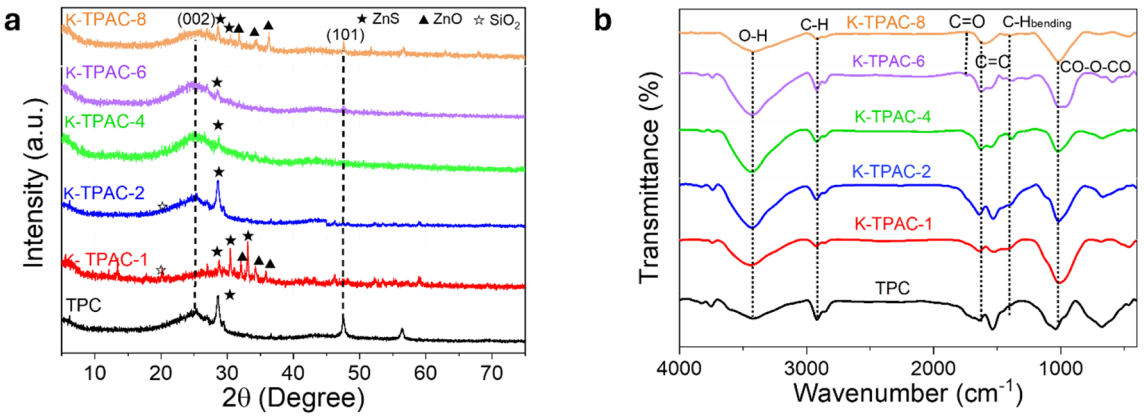

Fig. 2 **a** X-ray diffraction pattern and **b** FTIR of TPC and K-TPAC1-8

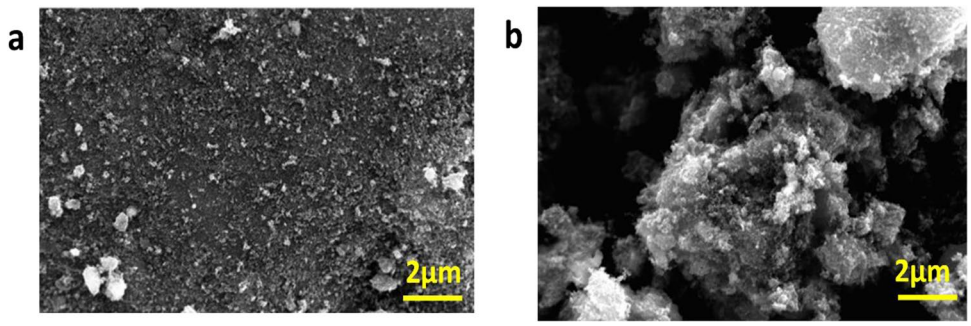

Fig. 3 SEM of images of **a** TPC and **b** K-TPAC6

The scanning electron microscope (SEM) (Fig. 3a, b) images clearly show the formation of cavities within the surface; the voids on the surface of the carbons appear to be the consequence of these chemical reagents evaporating during carbonization and its reaction with surface carbon, leaving the area that they had previously filled (Hu et al. 2022), which also explains the increase in surface area with the chemical activation of TPC.

The Brunauer–Emmett–Teller (BET) surface area of the K-TPAC-1, K-TPAC-2, K-TPAC-4, K-TPAC-6, and K-TPAC-8 are found to be 46, 45, 72, 154, 160, and 141 m^2/g respectively. An increase in the surface area of the adsorbent is noted up to treatment with 6 M KOH, after which it began to decrease. Other researchers also noticed a similar pattern in their investigations (Sirimuangjinda et al. 2013; Acosta et al. 2018). The reason might be that at very high concentrations of KOH, the wall between adjacent pores may rupture, leading to a decrease in the surface area.

The Helium Temperature-Programmed Decomposition (TPD) studies demonstrate the oxygen group contents on the surface of the adsorbent. Here, it is done to compare the functional groups on TPC and K-TPAC-6. Based on previous studies, it is assigned that carboxylic acids (will generate CO_2 gas below 673 K) and lactone (will generate CO_2 gas below 920 K), anhydrides (will generate CO_2 and CO above 873 K); ethers, phenols, quinones, and carbonyls (are responsible for CO evolution above 1000 K) (Boudou and Prent 2006; Manoj Kumar Reddy et al. 2015; Ibrahim Abouelamaiem et al. 2018). The TPD profiles of the adsorbents are shown in Fig. 4a and the data is given in Table 1. FTIR of K-TPAC-6 after He-TPD is taken to show that the oxygen functional groups have been eliminated due to the evolution of CO and CO_2 during TPD studies (Fig. S1). The total quantity of gas desorbed from the surface of K-TPAC-6 is more than the gas evolved from the TPC, which means that K-TPAC-6 has more oxygen functional groups than TPC. The increase in oxygen content can also be supported by FTIR and XPS.

According to the X-ray photoelectron spectroscopy (XPS) survey-wide scan, the oxygen atomic percentages in the TPC and K-TPAC-6 are 7.5% and 12.5% respectively, demonstrating oxygen content increase after activation (Fig. 4b). The defectiveness and oxidation status of the carbon on the adsorbent surface is assessed using XPS deconvolution peaks of C 1 s. The deconvolution peaks of carbon of the adsorbent in Fig. 4a show the peaks at different binding energies 284.1, 285.5, 286, and 288.6, and 290 eV. The peak at 284.1 eV belongs to C–C, C = C bonded carbons; the peak at 285.5 illustrates the defect carbon (Datsyuk et al. 2008; Shao et al. 2021). The peaks at 286, 288.6, and 290 eV belong to C–OH, C = O, and O-C = O (Shao et al. 2021). After activation, both the defect-rich carbon and carbon with oxygen functional group have been increased as shown in Fig. 4c.

The point of zero charge (pHPZC) is the pH where the surface of the adsorbent will be with no charge and above that pH adsorbent surface will have a negative charge and below that it will have a positive charge (Iheanacho et al. 2023). The pHPZC of TPC and K-TPAC-6 are 6.89 and 7.21 respectively (Fig. 4d); such type of increase in pHPZC in KOH-treated tire carbon was also observed in other studies (Acosta et al. 2018).

Adsorption studies

Comparison of adsorption efficiency for BPA removal by all the tire pyrolyzed activated carbons

The evaluation of the adsorption efficacy of all synthesized adsorbents is listed in Table 2. Removal efficiency of 84% was shown by K-TPAC-6, which was superior to that of TPC and other KOH-treated TPC adsorbents. The following studies were conducted using K-TPAC-6 adsorbent. The increased surface area of K-TPAC-6 led to an enhancement of defect-rich carbon in tire pyrolyzed carbon after KOH treatment, resulting in a larger adsorptive capacity.

To understand the equilibrium of adsorption, a series of adsorption experiments were conducted, whereby the adsorbent dosage and starting concentration of BPA and MB were varied. As the contact time increases, there is

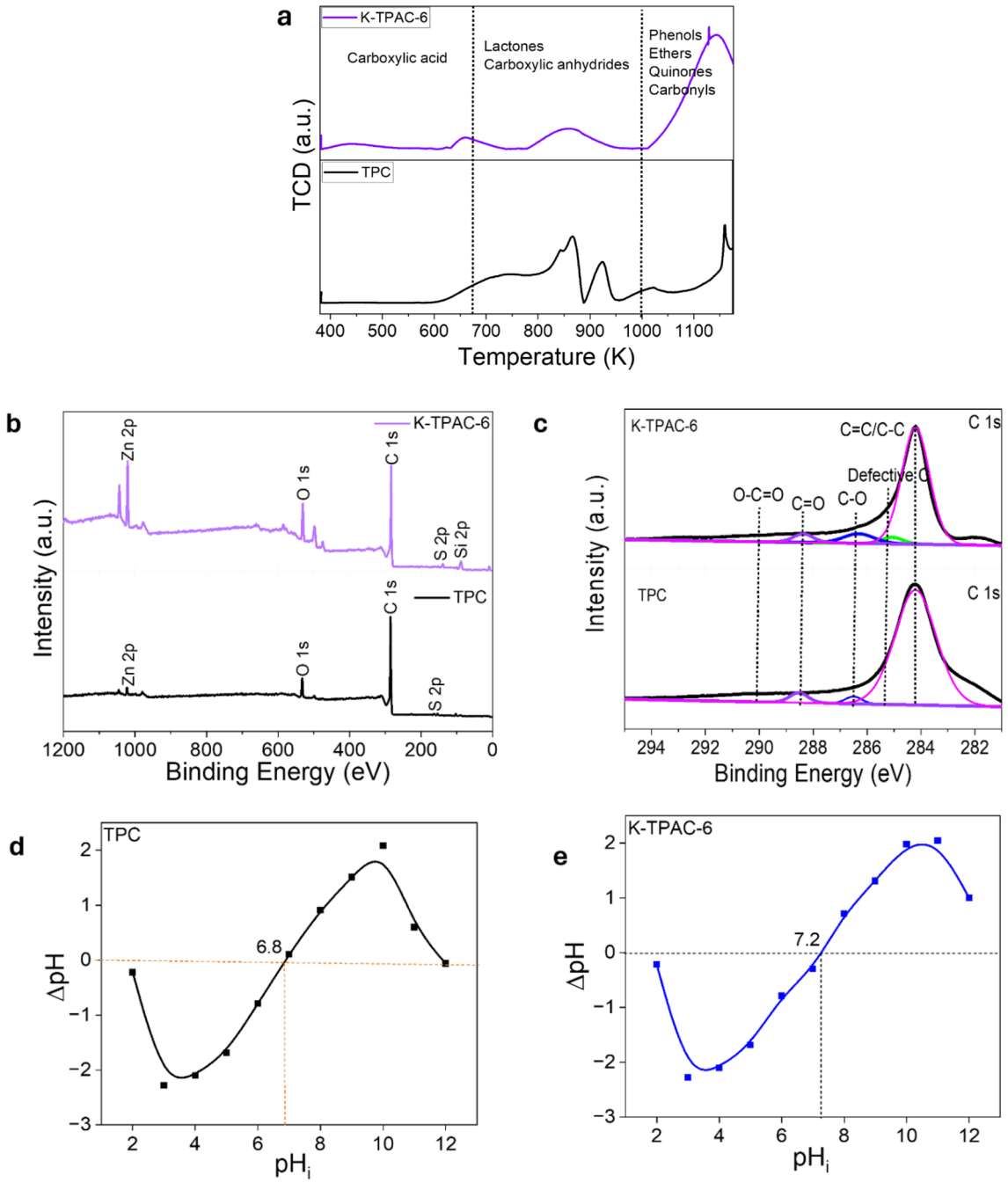

Fig. 4 **a** Temperature programmed decomposition studies. **b** XPS-Survey wide scan. **c** X-ray photoelectron spectra C1s deconvolution of TPC and K-TPAC-6. **d** pHPZC of TPC. **e** pHPZC of K-TPAC-6

a corresponding increase in the amount of BPA and MB adsorbed on the surface of the adsorbent until an equilibrium is reached. The adsorption using K-TPAC-6 has a higher efficiency, with equilibrium being achieved within 20 min. The results of the adsorption studies indicate that the initial concentration of the pollutant and the dose of the adsorbent significantly influence the efficacy of adsorption.

Effect of initial pollutant concentration and adsorbent dosage on adsorption efficiency of K-TPAC-6 for BPA and MB

Effect of initial pollutant concentration

The adsorption efficiency for BPA by K-TPAC-6 is 91% with a BPA solution with an initial concentration of 5 ppm,

Table 1 Temperature programmed decomposition studies and the quantity of CO or CO_2 gases evolved

Adsorbents	Peak position (K)	(CO&CO_2) mmol/g	Total gas evolved (CO&CO_2)
TPC	730	0.150	0.604 mmol/g
	866	0.204	
	924	0.063	
	1023	0.049	
	1609	0.138	
K-TPAC-6	440	0.020	0.747 mmol/g
	568	0.000	
	661	0.029	
	761	0.000	
	861	0.095	
	993	0.001	
	1129	0.602	

and it decreased to 57% as the concentration of pollutants increased from 5 to 75 ppm (Fig. 5a). The adsorption capacity has increased from 4.5 to 43.3 mg/g (Fig. 5b) (Table 3). Similarly, when the initial concentration of MB was 20 ppm, the effectiveness of MB removal is 99%.

However, this efficiency gradually reduced to 71% at a concentration of 200 ppm. Additionally, the q_e rose from 19.9 to 70.8 mg/g as the initial concentrations increased, as shown in Fig. 5d and Table 3. At high levels of BPA and MB (75 ppm and 100 ppm), there is a decrease in adsorption efficiency with the increase in pollutant concentration for both pollutants. As the adsorbent surface is overloaded at higher concentrations, the pollutant experiences incomplete adsorption, leftover with more unadsorbed molecules which decreases the adsorption efficiency. The adsorption capacity (q_e) is more at higher concentrations of pollutants. This is due to the excess availability of pollutant molecules at higher pollutant concentrations (Ezeh et al. 2017; Gorzin and Bahri Rasht Abadi 2018; Awad et al. 2019).

Table 2 Adsorption efficiency (%) for BPA by various adsorbents prepared

Sample	TPC	K-TPAC-1	K-TPAC-2	K-TPAC-4	K-TPAC-6	K-TPAC-8
Adsorption efficiency (%) for BPA	28	29	43	79	84	78
Adsorption capacity (mg/g)	5.6	5.8	8.6	15.8	16.8	15.6

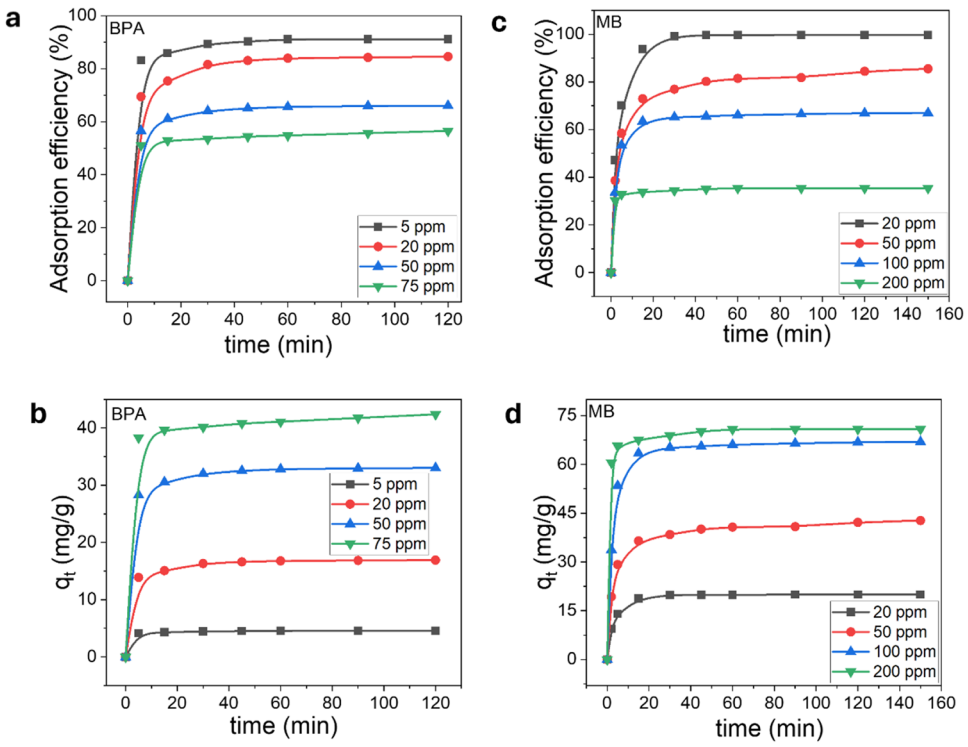

Fig. 5 Pollutant initial concentration effect on **a**, **b** adsorption efficiency and unit adsorption capacity for BPA removal and **c**, **d** adsorption efficiency and unit adsorption capacity for MB removal by K-TPAC-6

Table 3 Unit adsorption capacity (q_e) and adsorption efficiency (%) for BPA and MB adsorption on K-TPAC-6 with varying initial concentrations of pollutants

Initial BPA Concentration Effect			Initial MB Concentration effect		
BPA (ppm)	q_e (mg/g)	Adsorption efficiency (%)	MB (ppm)	q_e (mg/g)	Adsorption efficiency (%)
5	4.5	91	20	19.9	> 99
20	16.9	84	50	42.7	85
50	33.0	66	100	66.9	67
75	43.3	58	200	70.8	71

Effect of adsorbent dosage

As shown in Fig. 6a, the adsorption efficiency for BPA improved from 79 to 89% when the adsorbent dose was raised from 0.5 to 1.5 g/L. The unit adsorption capacity for 0.5 g/L of adsorbent was 31.5 mg/g, but it decreased to 11.8 mg/g for 1.5 g/L, as shown in Fig. 6b. Similarly, the adoption efficiency of MB increased from 86 to > 99% (Fig. 6c), while the adsorption capacity dropped from 34.4 to 13.3 mg/g for adsorbent dosages of 0.5 g/L and 1.5 g/L, respectively, as shown in Fig. 6d and Table 4.

As the total available surface area is more in the case of high adsorbent dosage, the adsorption efficiency is more (Gharbani et al. 2015). At the higher adsorbent dosage, the concentration of pollutant will become a limiting factor, leaving most of the active sites unsaturated or unadsorbed at equilibrium on the surface of the adsorbent; as a result, adsorption capacity q_e of the adsorbent decreases with increasing adsorbent dosage (Ezeh et al. 2017; Gorzin and Bahri Rasht Abadi 2018).

Kinetic study of adsorption

Studying kinetics is an important step to understand the adsorption of pollutants by adsorbent with respect to time. We can determine how quickly or slowly the adsorption is occurring. Three kinetic models are selected here; those are pseudo-first order, pseudo-second order, and intra-particle diffusion model.

The linear form of a pseudo-first-order can be expressed as follows with the Eq. (5):

$$\log\left(q_e - q_t\right) = \log q_e - \frac{k_1}{2.303}(t) \tag{5}$$

Here, q_e and q_t are the amount of pollutant adsorbed in mg/g of adsorbent at equilibrium and at time t respectively. The k_1 is the rate constant of adsorption (min^{-1}) (Lagergren 1898; Ho and McKay 1998; Yuh-Shan 2004; Huang et al. 2014; Gómez-Serrano et al. 2021). The plots of $\log\left(q_e - q_t\right)$ vs. t for various BPA (5, 20, 50, and 75 ppm) (Fig. 7a) and MB (20, 50, 100, and 200 ppm) (Fig. 7d) concentrations were used to compute the values of k_1(Table S1).

The equation for linear form for pseudo-second-order is represented with Eq. (6):

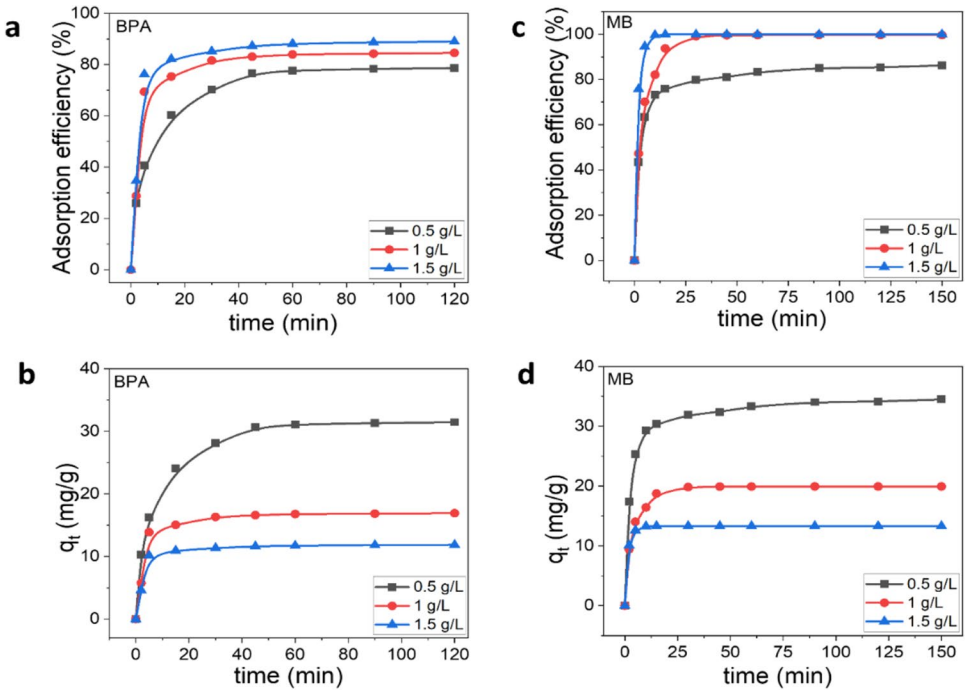

Fig. 6 Adsorbent dose effect on **a**, **b** adsorption efficiency and unit adsorption capacity for BPA removal and **c**, **d** adsorption efficiency and unit adsorption capacity for MB removal by K-TPAC-6

Table 4 Unit adsorption capacity (q_e) and adsorption efficiency (%) for BPA and MB adsorption on K-TPAC-6 with varying adsorbent dosage

Adsorbent dosage effect for BPA adsorption			Adsorbent dosage effect for MB adsorption		
Adsorbent dosage (g/L)	q_e (mg/g)	Adsorption efficiency (%)	Adsorbent dosage (g/L)	q_e (mg/g)	Adsorption efficiency (%)
0.5	31.5	79	0.5	34.4	86
1	16.9	84	1	19.9	> 99
1.5	11.8	89	1.5	13.3	> 99

$$\frac{t}{q_t} = \frac{1}{k_2 q_e} + \frac{1}{q_e}(t) \tag{6}$$

Here, q_e and q_t are the amount of pollutant adsorbed in mg/g of adsorbent at equilibrium and at time t respectively. The k_2 is the rate constant of second-order adsorption (g/mg/min) (Ho and McKay 1998, 1999; Gómez-Serrano et al. 2021).

The pseudo-2nd-order kinetics model exhibited the highest coefficient values, with an R^2 (correlation

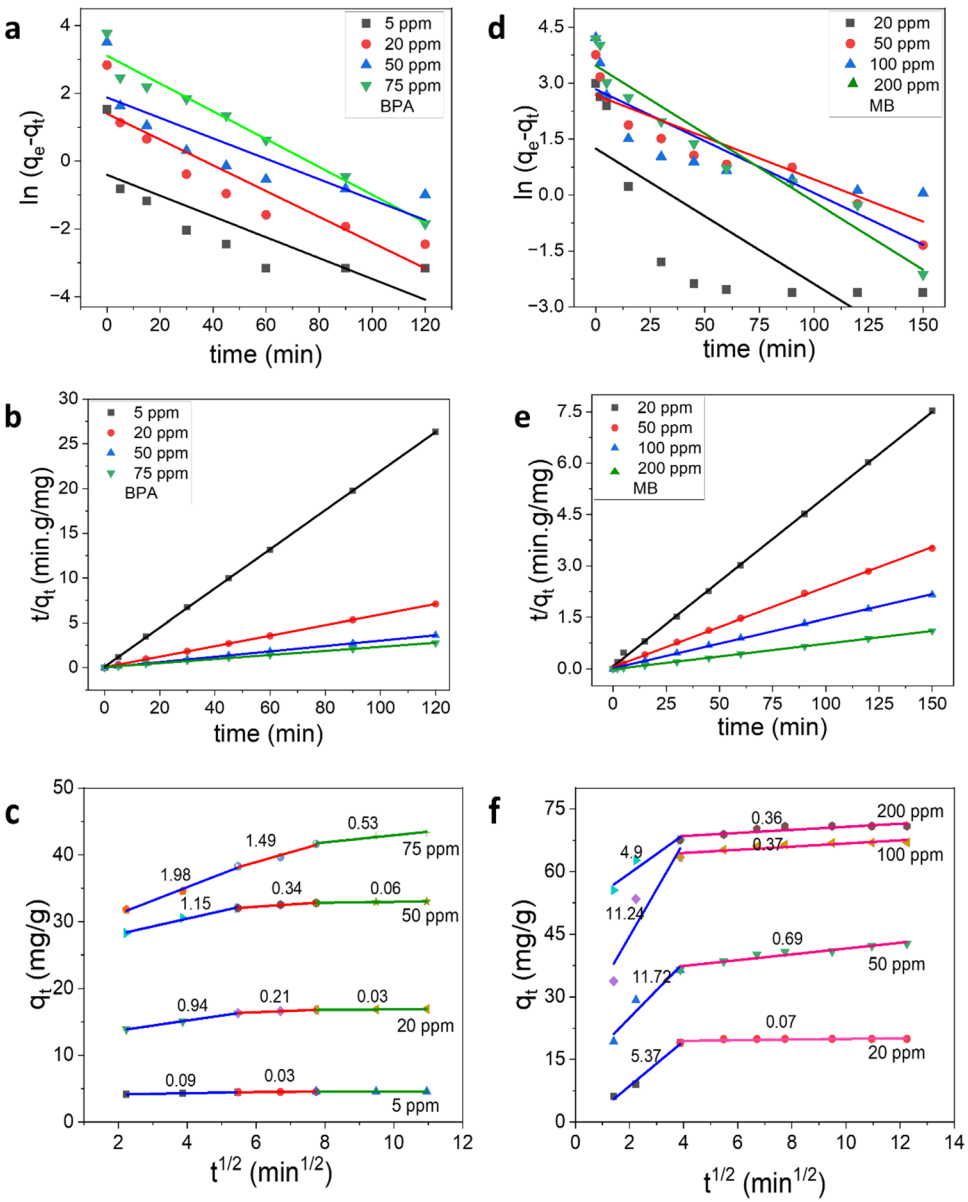

Fig. 7 **a** Pseudo-first order, **b** pseudo-second order, and **c** intra particle diffusion model fits for BPA adsorption with initial concentrations 5, 20, 50, and 75 ppm. **d** Pseudo-first-order, **e** pseudo-second-order, and **f** intra particle diffusion model fits for MB adsorption with initial concentrations 20, 50, 100, and 200 ppm by K-TPAC-6

Table 5 Pseudo-second-order kinetic parameters for BPA and MB removal by K-TPAC-6 with various initial concentrations

BPA					MB				
BPA Conc. (ppm)	q_e (mg/g)	q_e (mg/g) Experimental	k_2 (g/mg/min)	R^2	MB Conc. (ppm)	q_e (mg/g)	q_e (mg/g) Experimental	k_2 (g/mg/min)	R^2
5	4.6	4.7	2.4	0.99	20	20.2	19.9	28.9	0.99
20	17.0	17.0	17.9	0.99	50	42.8	42.7	98.6	0.99
50	33.4	41.2	26.7	0.99	100	68.5	68.0	90.5	0.99
75	43.5	44.0	129.1	0.99	200	83.3	70.8	28.2	0.99

coefficient) value 0.99. The findings presented in this study align with previous research on the adsorption of BPA (Javed et al. 2018; Ndagijimana et al. 2019) and MB (Hameed et al. 2007; Do et al. 2021) onto adsorbents. The theoretical values of k_2 and q_e were determined by analyzing the intercept and slope of the linear plot (t/q_t versus t for various concentrations of BPA (5–75 ppm) and MB (20–200 ppm) depicted in Fig. 7b and e. The results revealed a strong correlation between the calculated values and the experimental q_e values, as presented in Table 5.

To learn more about the rate-limiting stage in the adsorption process, the intra-particle diffusion model was utilized. Adsorption generally involves three stages (Rout et al. 2014): pollutant is transported by (1) film diffusion from the boundary film to the adsorbent's outer surface; (2) intra-particle diffusion from the adsorbent's surface to its pores; and (3) equilibrium stage adsorption of pollutant on the adsorbent's inner surface (Tang and Zhang 2016). The linear form of the Morris-weber Eq. (7) is:

$$q_{t=k_p t^{1/2}+C} \tag{7}$$

where q_t (mg/g) is the amount adsorbed within time t (min), k_p is the intra-particle diffusion rate constant (mg/g $min^{1/2}$), and C is the constant indicating the thickness of the boundary layer. In the plot of q_t vs. $t^{1/2}$, k_p is slope and C is the intercept (Weber and Morris 1963; Patawat et al. 2020). The higher the slope value, the more is the rate of adsorption (Huang et al. 2018). The intra-particle model fit for the adsorption kinetics with initial concentrations of 5, 20, 50, and 75 ppm of BPA and 20, 50, 100, and 200 ppm of MBwere drawn. The plots of q_t vs. $t^{1/2}$ (Fig. 7c and f) for both BPA and MB with all the concentrations are multilinear with different slopes, as these plots are not a straight single line indicate that intra-particle diffusion is not only rate-limiting step (Wang and Guo 2022). The first step slope has more in each case, which indicates that bulk diffusion is showing more adsorption rate than the intra-particle diffusion step (Huang et al. 2018).

Adsorption isotherms

The amount of pollutant adsorbed onto the adsorbent at equilibrium was studied and plotted as a function of the equilibrium concentration of a pollutant at constant temperature is considered as the adsorption isotherm. In this experiment, Langmuir and Freundlich's isotherms were used to evaluate experimental results.

Langmuir (1918) was first to propose this theory. It is based on certain assumptions: homogenous and fixed number of active sites on the surface of the adsorbent, monolayer adsorption of adsorbent molecules, and the adsorbed molecules do not interact (Do 1998; Ong et al. 2014).

Langmuir isotherm is expressed as in Eq. (8):

$$q_e = q_{max}\frac{K_L C_e}{1 + K_L C_e} \tag{8}$$

It can be rearranged as Eq. (9)

$$\frac{C_e}{q_e} = \frac{1}{q_{max K_L}} + \frac{C_e}{q_{max}} \tag{9}$$

Here, q_{max} (mg/g) is the maximum adsorption capacity and K_L (L/mg) Langmuir constant is related to the rate of adsorption. With the plot of $\frac{C_e}{qe}$ vsC_e (Fig. 11a), we will get an isotherm with the slope of ($1/q_{max}$) and intercept of ($1/(q_{max}{*}K_L)$). With this, we can predict q_{max} (mg/g) (Langmuir 1918; Elgeundi 1991; Zhuang et al. 2020; Mehrizad 2017).

Freundlich adsorption isotherms can be applied to multilayer adsorption on heterogeneous sites, in contrast to the Langmuir isotherm. It is predicted on the idea that affinities and the heat distribution of adsorption toward the heterogeneous surface are not uniform (Foo and Hameed 2010) and is represented with the Eq. (10).

$$q_e = K_F C^{\frac{1}{n}} \tag{10}$$

It can be rewritten as Eq. (11)

$$logq_e = logK_F + 1/nlogC_e \tag{11}$$

Here, the K_F is the Freundlich constant in mg/g and n is the Freundlich exponent. A higher n ($n > 1$) value indicates favorable adsorption (Mehrizad 2017; Zhuang et al. 2020).

The experimental data fits into Langmuir isotherm for BPA and MB adsorption with K-TPAC-6. Figure 8a and c (Table 6) is for linear Langmuir fits for BPA and MB and Fig. 8b and d (Table 6) is for linear Freundlich fits for BPA and MB. The q_{max} obtained from these Langmuir isotherms is 49.2 mg/g (with initial concentrations of 5, 20, 50, and 75 ppm of BPA), and 72.09 mg/g (with initial concentrations of 20, 50, 100, and 200 ppm of MB) at 298 K. These calculated values are similar to experimental values and the Langmuir isotherm plot exhibited the highest coefficient values than that of Freundlich isotherm.

Thermodynamic parameters

The study of the impact of temperature on the adsorption process can provide key information on entropy and enthalpy changes. The enthalpy change in chemisorption typically

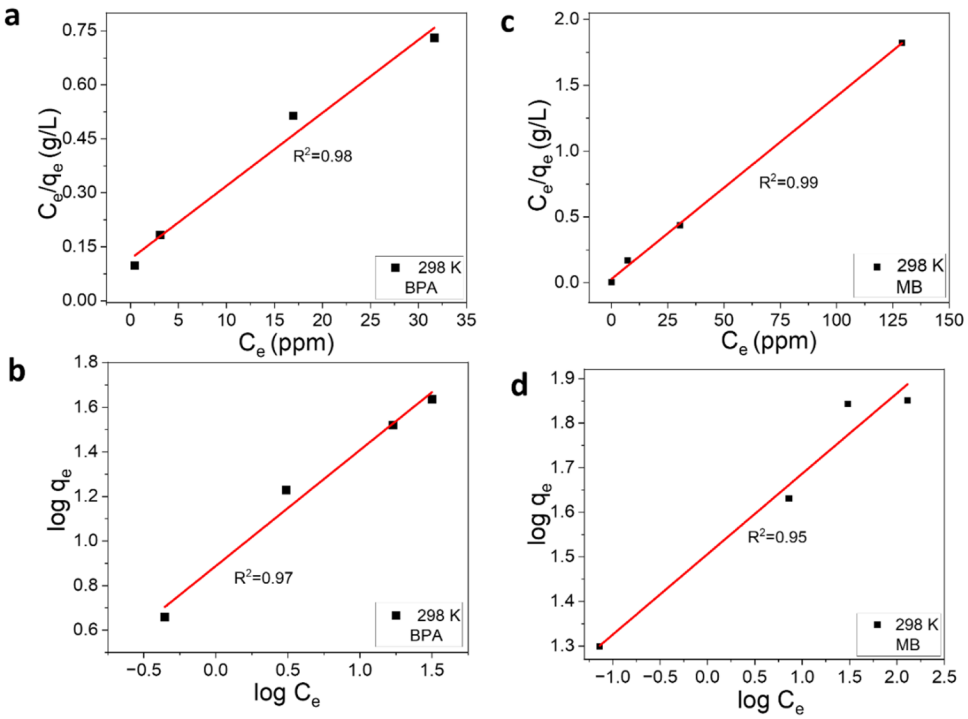

Fig. 8 **a**, **b** Langmuir and Freundlich fit for BPA adsorption at 298 K. **c**, **d** Langmuir and Freundlich for MB adsorption at 298 K

Table 6 Adsorption constants of Langmuir and Freundlich isotherms for BPA and MB removal by K-TPAC-6

Pollutant	Temperature (K)	Langmuir parameters			Freundlich parameters		
		q_{max}(mg/g)	K_L (L/mg)	R^2	n	K_F (mg/g)	R^2
BPA	298	49.2	0.174	0.98	1.93	7.73	0.97
MB	298	72.1	0.473	0.99	5.54	32.07	0.95

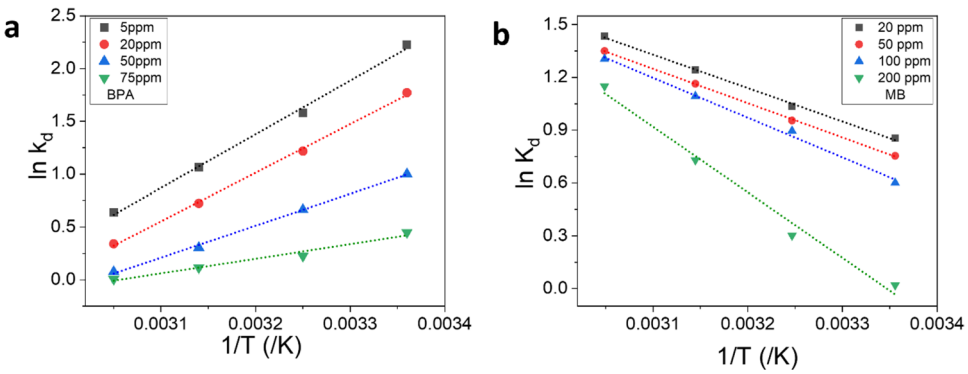

Fig. 9 Thermodynamic parameters for adsorption of **a** BPA with initial concentrations 5, 20, 50, and 75 ppm. **b** MB with initial concentration 20, 50, 100, 200 ppm at 298, 308, 318, and 328 K

Table 7 Thermodynamic parameters for BPA and MB removal by K-TPAC-6 at various temperatures with different initial pollutant concentrations

Pollutants	Initial concentration (ppm)	ΔH° (kJ/mol)	ΔS° (J/mol K)	ΔG° (kJ/mol)			
				298 K	308 K	318 K	328 K
BPA	5	−42.3	−123.7	−5.5	−4.0	−2.8	−1.7
	20	−38.7	−113.9	−4.3	−3.1	−1.9	−0.9
	50	−25.1	−76.1	−2.4	−1.7	−0.8	−0.2
	75	−11.5	−35.1	−1.1	−0.5	−0.3	−0.02
MB	20	15.5	59.2	−2.1	−2.6	−3.2	−3.9
	50	16.2	60.6	−1.8	−2.4	−3.0	−3.7
	100	18.8	68.1	−1.6	−2.2	−3.0	−3.6
	200	30.9	103.5	−0.1	−0.7	−1.0	−1.9

ranges from 80 to 200 kJ/mol, whereas the energy produced by physisorption is 2.1–20.9 kJ/mol (Üzek et al. 2022). The experiments were to know the effect of varying temperatures 298, 308, 318, and 328 K on the adsorption of BPA (5–75 ppm) and MB (20 ppm) by K-TPAC-6. To know the thermodynamic parameters (ΔG°, ΔH°, and ΔS°) are computed from the graph ln k_d vs. 1/T Eqs. (12, 13, and14) (Fig. 9a and Table 7).

$$k_d = \frac{q_e}{C_e} \tag{12}$$

$$\Delta G^o = RTlnk_d \tag{13}$$

$$lnk_d = -\frac{\Delta H^o}{R}\left(\frac{1}{T}\right) + \frac{\Delta S^o}{R} \tag{14}$$

where k_d is the equilibrium constant, q_e pollutant amount adsorbed, and C_e concentration of pollutant at equilibrium (Ratkowsky and Giles 1990; Mehrizad 2017).

The negative ΔH° value (−42.3 kJ/mol) for 5 ppm BPA adsorption indicates it is an exothermic process, and this change in enthalpy is found to decrease (−38.7, −25.1, and −11.5 kJ/mol) with the increased initial concentrations (20, 50, and 75 ppm). Thus, the exothermic nature is more for lower concentrated BPA solution as the most energetic sites are indeed filled first at low BPA concentrations (Acosta et al. 2018). Such type of enthalpy change range is also observed by many other researchers for different pollutants (Saleh et al. 2017; Tran et al. 2017; Hu et al. 2022). The values of entropy ΔS° changes are negative indicating that the randomness has been decreased as the pollutant particles moment is arrested as they were adsorbed on the surface of adsorbents. The negative value of Gibb's free energy ΔG° gives information about the spontaneous process.

The positive ΔH° (15.5 kJ/mol) value for 20 ppm MB solution indicates the endothermic nature of MB adsorption on K-TPAC-6. The values of enthalpy change ΔH° and the entropy change ΔS° for all initial concentrations of MB solution are positive and shown in Fig. 9b and Table 7. The positive values of enthalpy is because of the dissociation of dye to give monomer from dimer or aggregates before it get adsorbed by adsorbent (Dural et al. 2011). In the process of MB adsorption, the positive value of ΔS° indicates that there is a rise in randomness at the interface between the adsorbent and the liquid, which may be accompanied by structural changes or interactions between the molecules of MB and activated Carbon (Bedin et al. 2016). The positive values of ΔH° and ΔS° are also observed by other scientists (Bhattacharyya and Sharma 2005; Hong et al. 2009; Makrigianni et al. 2015; Bedin et al. 2016; Egbosiuba et al. 2020). The Gibbs free energy change ΔG° values are negative indicating the spontaneous nature of adsorption. The thermodynamic parameters of MB adsorption are shown in Fig. 9b and Table 7.

Effect of pH on adsorption of BPA and MB

The K-TPAC-6 has better adsorption efficiency for BPA for a wider range of pH until pH 9. The adsorption efficiency from pH 2 to 9 is shown as 78% to 84% from pH

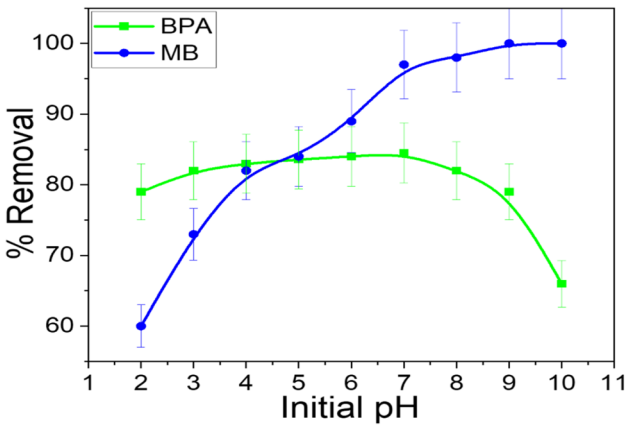

Fig. 10 Effect of initial pH on adsorption of BPA and MB by K-TPAC-6

2 to 9. However, at higher pH-10, the adsorption is eventually decreased to 65%. This fashion is also found by Bautista-Toledo et al. (2005). One plausible explanation for this phenomenon is that BPA is in its molecular state while the pH was below 8.0, so there is no influence of pH for the maximum range of pH as shown in (Fig. 10). Then, the process of deprotonation occurred initially, and subsequently at about pH levels 8.0 and 9.0 respectively, resulting in the formation of mono or divalent anions. The decrease in BPA removal was found at higher (pH-10) levels, possibly because of the repulsive electrostatic interactions between the negatively charged surface of the adsorbents and the bisphenolate anion (Bhatnagar and Anastopoulos 2017).

There is a significant variation in the adsorption of MB at different pH levels. At a lower pH below 7, the adsorption efficiency of MB is less, which indicates the influence of pH on its adsorption. This may be because the surface of the adsorbent and MB molecule both will have a positive charge at lower pH. The removal of MB increases drastically at higher pH (Wang et al. 2005; Malarvizhi and Ho 2010) and attained more than 99% removal. It is because the adsorbent surface has a negative charge which favors the adsorption of MB (Fig. 10). That means there exists electrostatic interactions between pollutant and adsorbent (Kavitha and Namasivayam 2007; Ramaraju et al. 2014; Manoj Kumar Reddy et al. 2015).

Effect of added salt NaCl on the BPA and MB adsorption

The ion effect was conducted for the presence of 1, 5, and 10 mM NaCl along with pollutant to observe their interference with pollutants adsorption by adsorbent. These ions have the capability of hindering the electrostatic interactions of the pollutant with the adsorbent, as they can be involved in those interactions. These ions can also hinder the hydrogen bonding of pollutants with adsorbent by salting out the -OH groups of adsorbents. The K-TPAC-6 has shown an adsorption efficiency of approximately 84% (Fig. 11a) (Table S2) in the presence of all the different molar concentrations of NaCl. There is no effect of these ions presence on the adsorption of BPA. It may indicate that there is no major role of electrostatic interaction or H-bonding in the adsorption of BPA (Shao et al. 2021) by K-TPAC-6.

The MB adsorption decreased with increased NaCl concentrations. As the NaCl concentration increased from 1 to 10 mM, its adsorption decreased from 99 to 87% as shown in Fig. 11b and Table S2. This fashion of decreasing adsorption of MB in the presence of electrolytes is also seen by Boumediene et al. (2018) and Ali et al. (2019) in their research. It shows that electrostatic interactions play a major role in the adsorption of MB.

Desorption and reusability

The desorption of BPA was done with ethanol as it is found to be a promising desorbing agent rather than HCl, NaCl, and NaOH

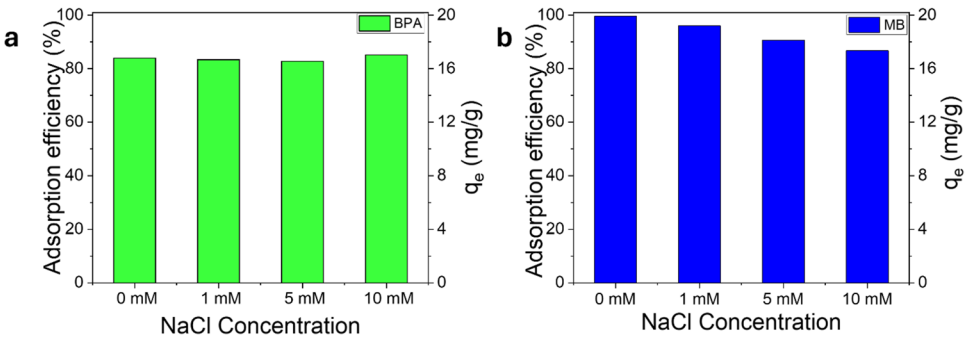

Fig. 11 Adsorption efficiencies **a** for BPA and **b** for MB at different ionic concentrations

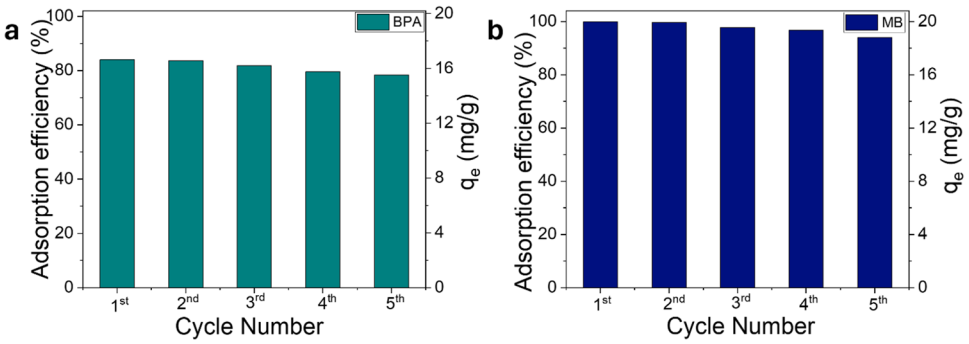

Fig. 12 Adsorption efficiencies **a** for BPA and **b** for MB after each cycle by K-TPAC-6

Table 8 Comparison with the literature for BPA adsorption

Adsorbent	Adsorption capacity (mg/g)	Pollutant initial concentration	Adsorbent dose	Equilibrium time	Isotherm model		Reference
CTAB functionalized walnut shell	38.5	10–200 ppm	1 g/L	6 h	Langmuir isotherm	297 K	Dovi et al. (2021)
17 α ethinyl estradiol on SWCNT	13.4	1 µm	0–50 mg/L	4 h	Langmuir isotherm l		Joseph et al. (2011)
RHA	8.6	10–400 mg/L	30 mg/L	120 min	Langmuir isotherm	288 K	Sudhakar et al. (2016)
	8.7					303 K	
	10.5					318 K	
GAC	3.1	10–400 mg/L	20 mg/L	120 min		288 K	
	3.5					303 K	
	3.8					318 K	
MIP	16.81	5–120 mg/L	1 g/L	60 min	Langmuir isotherm	298 K	Xie et al. (2019)
SB functionalized fiber	4.86	10–30 mg/L	10–20 g/L	60 min	Langmuir isotherm	293 K	Tursi et al. (2018)
Coir pith-acid treated	4.3	20 ppm	1 g/L	38 h	R.T		Lazim et al. (2015)
Coconut shell-acid treated	4.1						
Banana bunches-acid treated	4.1						
K-TPAC-6	49.2	5–75 ppm	1 g/L	30 min	Langmuir isotherm	298 K	Present study

solutions. The desorption was made with MB 0.5 M HCl, which was found to be more suitable than other solvents. In acidic conditions, the adsorbent surface becomes positive, where the MB can be effectively desorbed. The regenerated adsorbent shows considerable efficiency even in the fifth cycle for both BPA and MB adsorption independently (Fig. 12 a and b) (Table S3).

Table 9 Comparison with the literature for MB adsorption

Adsorbent	Adsorption capacity (mg/g)	Pollutant initial concentration	Adsorbent dosage	Equilibrium time	Isotherm model	Reference
Sour soup (sodium hypochlorite sanitized)	55.3	100–250 ppm	5 g/L	200 min	Langmuir isotherm	Meili et al. (2019)
Bagasse (sodium hypochlorite sanitized)	17.4	50–200 ppm				
NATPC	53.1	5–150 ppm	2 g/L	60 min	Langmuir isotherm 293 K	Wang et al. (2014)
AC-CO_2	45.9	5–150 ppm	1 g/L	72 h	R.T	Mohd Shaid et al. (2017)
AC-$ZnCl_2$	17.8					
AC-Char	34.8					
Rice husk C-steam + O_3 activation	24.8	10–30 ppm	1 g/L	75 min	Langmuir isotherm 298 K	Manoj Kumar Reddy et al. (2015)
Rice husk C-CO_2 + O_3 activation	26.2					
Rice husk C-steam + CO_2 + O_3 activation	27.8					
Clin/Fe_3O_4	45.6	10–50 ppm	1 g/L	60 min	Langmuir isotherm 298 K	Noori et al. (2022)
Alg/Clin/Fe_3O_4	12.4		2 g/L			
K-TPAC-6	72.1	20–200 ppm	1 g/L	15 min	Langmuir isotherm 298 K	Present study

Plausible mechanism

The tests, including the presence of NaCl (Fig. 11a) and the influence of pH (Fig. 10) on BPA adsorption, suggest that there is no significant effect of electrostatic interactions or hydrogen bonding. From XPS, it was confirmed that KOH treatment leads to defective carbon improvement in the adsorbent and based on the literature, we assume hydrophobic interactions (Sun et al. 2020; Shao et al. 2021) or π-π interactions (Sun et al. 2020) play a significant role in the adsorption of BPA by K-TPAC-6 (Shao et al. 2021), whereas the hydrogen bonding contribution is minimal. In the SEM images of adsorbent after BPA adsorption, we can observe the aggregation on its surface (Fig. S2).

As the presence of NaCl in MB solution (Fig. 11b) and the initial pH (Fig. 10) can affect the MB adsorption efficiency, this indicates the major role of electrostatic interactions and hydrogen bonding between MB and K-TPAC-6 adsorbent (Abdulhameed et al. 2021; Hanjing Xue a,1 et al. 2021; Dolas 2023), along with a small portion of π-π interactions. This can be explained by analyzing the FTIR of the adsorbent before and after MB adsorption (Fig. S3). The band at 3420 cm^{-1} in activated carbon (K-TPAC-6) shifted to 3440 cm^{-1} after MB adsorption (K-TPAC-6-MB), as the stretching vibration of O–H combined with the N–H stretching vibration (Pezoti et al. 2014). The peak at 1630 cm^{-1} is assigned to N–H bending vibration coupled with C-N and the decrease in intensity of peaks in the region of 800 to 500 cm^{-1} indicates π-π interactions between adsorbent and MB (Fu et al. 2015; Bedin et al. 2016).

The comparative study for the adsorption capacities of BPA and MB by K-TPAC-6 with the literature is shown in Tables 8 and 9 respectively.

Conclusions

The best adsorbent selected is K-TPAC-6 which has a surface area 160 m^2/g. It has shown 84% and > 99% removal for BPA and MB respectively, with initial pollutant concentration of 20 ppm. The enhanced BPA removal can be explained by improved defect-rich carbon and surface area (BET and XPS), which provides sites for hydrophobic and π-π interactions between K-TPAC-6 adsorbent and BPA pollutant. The high adsorption of MB is because of improved oxygen-containing groups (XPS, FTIR, and He-TPD) on the K-TPAC-6 surface, which are helpful for MB adsorption with electrostatic interactions and hydrogen bonding. The adsorption of BPA is exothermic and that is endothermic for MB. Neither NaCl presence nor initial pH affects the BPA adsorption, but they can do so for MB adsorption. Adsorption of both the pollutants followed pseudo-second-order kinetics and Langmuir isotherm model. And efficiency of the adsorbent is notable even in 5th cycle. Hence, it is proved that the waste tire is a promising source to synthesize activated carbon, which can show good adsorption efficiency for both BPA and MB from aqueous streams.

The fundamental findings observed in this study can be the basis for future studies on the simultaneous adsorption of these two pollutants (BPA and MB), which is very much essential for present society as the co-existence of endocrine-disrupting chemicals (BPA) and cationic dye (MB) is common in wastewater.

Supplementary Information The online version contains supplementary material available at https://doi.org/10.1007/s11356-024-34698-5.

Acknowledgements Shiva Deepti Rangu is thankful to Indian Institute of Technology, Hyderabad, for providing instruments and lab facilities and also to Commissioner of Collegiate Education, Telangana, and Tara Government College(A),Sangareddy for granting permission and providing support.

Author contribution Shiva Deepti Rangu: writing—original draft, visualization, methodology, formal analysis, investigation. Harsha S. Rangappa: methodology, formal analysis, investigation. Phyu Phyu Mon: methodology, review, and editing. Phyu Phyu Cho: Formal analysis. Umamaheswara Rao Mudadla: formal analysis. Subrahmanyam Challapalli: conceptualization, resources, writing—original draft, review and editing, supervision, and project administration. All the authors read and approved the final manuscript.

Funding No funding was received.

Data availability Supporting data is provided in the manuscript.

Declarations

Ethics approval Not applicable.

Consent to participate All authors contributed to this work.
Consent for publication All authors have approved authorship, read, and consented to publication.

Competing interests The authors declare no competing interests.

References

Abdulhameed AS, Firdaus Hum NNM, Rangabhashiyam S et al (2021) Statistical modeling and mechanistic pathway for methylene blue dye removal by high surface area and mesoporous grass-based activated carbon using K_2CO_3 activator. J Environ Chem Eng 9:105530. https://doi.org/10.1016/j.jece.2021.105530

Abrams CF, Kremer K (2003) Combined coarse-grained and atomistic simulation of liquid bisphenol A–polycarbonate: liquid packing and intramolecular structure. Macromolecules 36:260–267. https://doi.org/10.1021/ma0213495

Acosta R, Nabarlatz D, Sánchez-Sánchez A et al (2018) Adsorption of bisphenol A on KOH-activated tyre pyrolysis char. J Environ Chem Eng 6:823–833. https://doi.org/10.1016/j.jece.2018.01.002

Ali I, Mohd A, Khan TA (2012) Low cost adsorbents for the removal of organic pollutants from wastewater. J Environ Manage 113:170–183. https://doi.org/10.1016/j.jenvman.2012.08.028

Ali SA, Yaagoob IY, Mazumder MAJ, Al-Muallem HA (2019) Fast removal of methylene blue and Hg(II) from aqueous solution using a novel super-adsorbent containing residues of glycine and maleic acid. J Hazard Mater 369:642–654. https://doi.org/10.1016/j.jhazmat.2019.02.082

Awad AM, Shaikh SMR, Jalab R et al (2019) Adsorption of organic pollutants by natural and modified clays: a comprehensive review. Sep Purif Technol 228:115719. https://doi.org/10.1016/j.seppur.2019.115719

Bautista-Toledo I, Ferro-García MA, Rivera-Utrilla J et al (2005) Bisphenol A removal from water by activated carbon. Effects of carbon characteristics and solution chemistry. Environ Sci Technol 39:6246–6250. https://doi.org/10.1021/es0481169

Bedin KC, Martins AC, Cazetta AL et al (2016) KOH-activated carbon prepared from sucrose spherical carbon: adsorption equilibrium, kinetic and thermodynamic studies for Methylene Blue removal. Chem Eng J 286:476–484. https://doi.org/10.1016/j.cej.2015.10.099

Bhatnagar A, Anastopoulos I (2017) Adsorptive removal of bisphenol A (BPA) from aqueous solution: a review. Chemosphere 168:885–902. https://doi.org/10.1016/j.chemosphere.2016.10.121

Bhattacharyya K, Sharma A (2005) Kinetics and thermodynamics of Methylene Blue adsorption on Neem () leaf powder. Dyes Pigments 65:51–59. https://doi.org/10.1016/j.dyepig.2004.06.016

Boudou JP (2006) Prent P (2006) Nitrogen in aramid-based activated carbon fibres by XPS. TPD and XANES Carbon 44(12):2452–2462. https://doi.org/10.1016/j.carbon.2006.04.036

Boumediene M, Benaïssa H, George B et al (2018) Effects of pH and ionic strength on methylene blue removal from synthetic aqueous solutions by sorption onto orange peel and desorption study. J Mater Env Sci 9:1700–1711. https://doi.org/10.26872/jmes.2018.9.6.190

Careghini A, Mastorgio AF, Saponaro S, Sezenna E (2015) Bisphenol A, nonylphenols, benzophenones, and benzotriazoles in soils, groundwater, surface water, sediments, and food: a review. Environ Sci Pollut Res 22:5711–5741. https://doi.org/10.1007/s11356-014-3974-5

Chen S, Tao Y, Wang P et al (2023) Association of urinary bisphenol A with cardiovascular and all-cause mortality: National Health and Nutrition Examination Survey (NHANES) 2003–2016. Environ Sci Pollut Res 30:51217–51227. https://doi.org/10.1007/s11356-023-25924-7

Dandekar A, Baker RTK, Vannice MA (1998) Characterization of activated carbon, graphitized carbon fibers and synthetic diamond powder using TPD and DRIFTS. Carbon 36:1821–1831. https://doi.org/10.1016/S0008-6223(98)00154-7

Datsyuk V, Kalyva M, Papagelis K et al (2008) Chemical oxidation of multiwalled carbon nanotubes. Carbon 46:833–840. https://doi.org/10.1016/j.carbon.2008.02.012

Do DD (1998) Adsorption analysis: equilibria and kinetics (with Cd containing computer Matlab programs). World Scientific

Do TH, Nguyen VT, Dung NQ et al (2021) Study on methylene blue adsorption of activated carbon made from Moringa oleifera leaf. Mater Today Proc 38:3405–3413. https://doi.org/10.1016/j.matpr.2020.10.834

Dolas H (2023) Activated carbon synthesis and methylene blue adsorption from pepper stem using microwave assisted impregnation method: Isotherm and kinetics. J King Saud Univ - Sci 35:102559. https://doi.org/10.1016/j.jksus.2023.102559

Dovi E, Kani AN, Aryee AA et al (2021) Decontamination of bisphenol A and Congo red dye from solution by using CTAB functionalised walnut shell. Environ Sci Pollut Res 28:28732–28749. https://doi.org/10.1007/s11356-021-12550-4

Dural MU, Cavas L, Papageorgiou SK, Katsaros FK (2011) Methylene blue adsorption on activated carbon prepared from Posidonia oceanica (L.) dead leaves: Kinetics and equilibrium studies. Chem Eng J 168:77–85. https://doi.org/10.1016/j.cej.2010.12.038

Egbosiuba TC, Abdulkareem AS, Kovo AS et al (2020) Ultrasonic enhanced adsorption of methylene blue onto the optimized surface area of activated carbon: Adsorption isotherm, kinetics and thermodynamics. Chem Eng Res Des 153:315–336. https://doi.org/10.1016/j.cherd.2019.10.016

Elgeundi M (1991) Colour removal from textile effluents by adsorption techniques. Water Res 25:271–273. https://doi.org/10.1016/0043-1354(91)90006-C

Erkekoglu P, Koçer-Gümüşel B (2017) Bisphenol A: exposure and health risks. BoD – Books on Demand

Ezeh K, Ogbu IC, Akpomie KG et al (2017) Utilizing the sorption capacity of local Nigerian sawdust for attenuation of heavy metals from solution: isotherm, kinetic, and thermodynamic investigations. Pac J Sci Technol 18:251–264. https://www.researchgate.net/publication/317663559

Ferdosian F (2015) Synthesis, characterization and applications of lignin-based epoxy resins. University of Western Ontario, School of Graduate and Postdoctoral Studies

Foo KY, Hameed BH (2010) Insights into the modeling of adsorption isotherm systems. Chem Eng J 156:2–10. https://doi.org/10.1016/j.cej.2009.09.013

Frikha K, Limousy L, Pons Claret J et al (2022) Potential valorization of waste tires as activated carbon-based Adsorbent for organic contaminants removal. Materials 15:1099. https://doi.org/10.3390/ma15031099

Fu J, Chen Z, Wang M et al (2015) Adsorption of methylene blue by a high-efficiency adsorbent (polydopamine microspheres): Kinetics, isotherm, thermodynamics and mechanism analysis. Chem Eng J 259:53–61. https://doi.org/10.1016/j.cej.2014.07.101

Gharbani P, Mehrizad A, Jafarpour I (2015) Adsorption of penicillin by decaffeinated tea waste. Pol J Chem Technol 17:95–99. https://doi.org/10.1515/pjct-2015-0056

Gharbani P, Mehrizad A, Mosavi SA (2022) Optimization, kinetics and thermodynamics studies for photocatalytic degradation of Methylene Blue using cadmium selenide nanoparticles. Npj Clean Water 5:34. https://doi.org/10.1038/s41545-022-00178-x

Gómez-Serrano V, Adame-Pereira M, Alexandre-Franco M, Fernández-González C (2021) Adsorption of bisphenol A by activated carbon developed from PET waste by KOH activation. Environ Sci Pollut Res 28:24342–24354. https://doi.org/10.1007/s11356-020-08428-6

Gorzin F, Bahri Rasht Abadi M (2018) Adsorption of Cr(VI) from aqueous solution by adsorbent prepared from paper mill sludge: Kinetics and thermodynamics studies. Adsorpt Sci Technol 36:149–169. https://doi.org/10.1177/0263617416686976

Gupta VK, Carrott PJM, Ribeiro Carrott MML, Suhas (2009) Low-cost adsorbents: growing approach to wastewater treatment—a review. Crit Rev Environ Sci Technol 39:783–842. https://doi.org/10.1080/10643380801977610

Hafezi SA, Abdel-Rahman WM (2019) The endocrine disruptor bisphenol A (BPA) exerts a wide range of effects in carcinogenesis and response to therapy. Curr Mol Pharmacol 12:230–238. https://doi.org/10.2174/1874467212666190306164507

Hameed B, Din A, Ahmad A (2007) Adsorption of methylene blue onto bamboo-based activated carbon: kinetics and equilibrium studies. J Hazard Mater 141:819–825. https://doi.org/10.1016/j.jhazmat.2006.07.049

Ho YS, McKay G (1998) Sorption of dye from aqueous solution by peat. Eng J 70:115–124. https://doi.org/10.1016/S0923-0467(98)00076-1

Ho YS, McKay G (1999) Pseudo-second order model for sorption processes. Process Biochem 34:451–465. https://doi.org/10.1016/S0032-9592(98)00112-5

Hong S, Wen C, He J et al (2009) Adsorption thermodynamics of Methylene Blue onto bentonite. J Hazard Mater 167:630–633. https://doi.org/10.1016/j.jhazmat.2009.01.014

Hu C, Hu S, Fang P et al (2022) Waste-tire-derived activated carbon as efficient adsorbent of P-nitrophenol from wastewater. J Chem 2022:1–12. https://doi.org/10.1155/2022/7313899

Huang W-Y, Li D, Liu Z-Q et al (2014) Kinetics, isotherm, thermodynamic, and adsorption mechanism studies of $La(OH)_3$ -modified exfoliated vermiculites as highly efficient phosphate adsorbents. Chem Eng J 236:191–201. https://doi.org/10.1016/j.cej.2013.09.077

Huang Y, Lee X, Grattieri M et al (2018) A sustainable adsorbent for phosphate removal: modifying multi-walled carbon nanotubes with chitosan. J Mater Sci 53:12641–12649. https://doi.org/10.1007/s10853-018-2494-y

Ibrahim Abouelamaiem D, Mostazo-López MJ, He G et al (2018) New insights into the electrochemical behaviour of porous carbon electrodes for supercapacitors. J Energy Storage 19:337–347. https://doi.org/10.1016/j.est.2018.08.014

Iheanacho OC, Nwabanne JT, Obi CC et al (2023) Adsorptive dephenolization of aqueous solutions using thermally modified corn cob: mechanisms, point of zero charge, and isosteric heat studies. Adsorpt Sci Technol 2023:1–14. https://doi.org/10.1155/2023/2813663

Javed H, Luong DX, Lee C-G et al (2018) Efficient removal of bisphenol-A by ultra-high surface area porous activated carbon derived from asphalt. Carbon 140:441–448. https://doi.org/10.1016/j.carbon.2018.08.038

Jia B, Shi T, Li Z et al (2019) Toxicological effects of bisphenol A exposure-induced cancer cells migration via activating directly integrin β1. Chemosphere 220:783–792. https://doi.org/10.1016/j.chemosphere.2018.12.120

Joseph L, Heo J, Park Y-G et al (2011) Adsorption of bisphenol A and 17α-ethinyl estradiol on single walled carbon nanotubes from seawater and brackish water. Desalination 281:68–74. https://doi.org/10.1016/j.desal.2011.07.044

Kavitha D, Namasivayam C (2007) Experimental and kinetic studies on methylene blue adsorption by coir pith carbon. Bioresour Technol 98:14–21. https://doi.org/10.1016/j.biortech.2005.12.008

Kumar R, Qureshi M, Vishwakarma DK et al (2022) A review on emerging water contaminants and the application of sustainable removal technologies. Case Stud Chem Environ Eng 6:100219. https://doi.org/10.1016/j.cscee.2022.100219

Kuśmierek K, Świa A, Cherbański R, Molga E (2020) Adsorption of bisphenol a from aqueous solutions by activated tyre pyrolysis char—effect of physical and chemical activation. Chem Process Eng 2:129–141. https://doi.org/10.24425/cpe.2020.132536

Lagergren S (1898) ZUR Theorie Der Sogenannten Adsorption Geloster Stoffe. 24:1–39

Langmuir I (1918) The adsorption of gases on plane surfaces of glass, mica and platinum. J Am Chem Soc 40:1361–1403. https://doi.org/10.1021/ja02242a004

Lazim ZM, Hadibarata T, Puteh MH, Yusop Z (2015) Adsorption characteristics of bisphenol A onto low-cost modified phyto-waste material in aqueous solution. Water Air Soil Pollut 226:34. https://doi.org/10.1007/s11270-015-2318-5

Machin EB, Pedroso DT, De Carvalho JA (2017) Energetic valorization of waste tires. Renew Sustain Energy Rev 68:306–315. https://doi.org/10.1016/j.rser.2016.09.110

Makrigianni V, Giannakas A, Deligiannakis Y, Konstantinou I (2015) Adsorption of phenol and methylene blue from aqueous solutions by pyrolytic tire char: equilibrium and kinetic studies. J Environ Chem Eng 3:574–582. https://doi.org/10.1016/j.jece.2015.01.006

Malarvizhi R, Ho Y-S (2010) The influence of pH and the structure of the dye molecules on adsorption isotherm modeling using activated carbon. Desalination 264:97–101. https://doi.org/10.1016/j.desal.2010.07.010

Manoj Kumar Reddy P, Krushnamurty K, Mahammadunnisa SK et al (2015) Preparation of activated carbons from bio-waste: effect of surface functional groups on methylene blue adsorption. Int J Environ Sci Technol 12:1363–1372. https://doi.org/10.1007/s13762-014-0506-2

Mehrizad A (2017) Adsorption studies of some phenol derivatives onto Ag-cuttlebone nanobiocomposite: modeling of process by response surface methodology. Res Chem Intermed 43:4295–4310. https://doi.org/10.1007/s11164-017-2874-y

Mehrizad A, Gharbani P (2016) Removal of methylene blue from aqueous solution using nano-TiO_2/UV process: optimization by response surface methodology. Prog Color Colorants Coat 9:135–143. https://doi.org/10.30509/PCCC.2016.75878

Mehrizad A, Aghaie M, Gharbani P et al (2012) Comparison of 4-chloro-2-nitrophenol adsorption on single-walled and multi-walled carbon nanotubes. Iran J Environ Health Sci Eng 9:5. https://doi.org/10.1186/1735-2746-9-5

Mehrizad A, Gharbani P (2014) Decontamination of 4-Chloro-2-nitrophenol from aqueous solution by graphene adsorption: equilibrium, kinetic, and thermodynamic studies. Pol J Environ Stud 23. https://doi.org/10.15244/pjoes/26779

Meili L, Lins PVS, Costa MT et al (2019) Adsorption of methylene blue on agroindustrial wastes: experimental investigation and phenomenological modelling. Prog Biophys Mol Biol 141:60–71. https://doi.org/10.1016/j.pbiomolbio.2018.07.011

MohdShaid MSH, Ahmad Zaini MA, Nasri NS (2017) Isotherm studies of methylene blue adsorption onto waste tyre pyrolysis powder-based activated carbons. Malays J Fundam Appl Sci 13:671–675. https://doi.org/10.11113/mjfas.v13n4.924

Mopoung S, Dejang N (2021) Activated carbon preparation from eucalyptus wood chips using continuous carbonization–steam activation process in a batch intermittent rotary kiln. Sci Rep 11:13948. https://doi.org/10.1038/s41598-021-93249-x

Mpatani FM, Aryee AA, Kani AN et al (2020) Uptake of micropollutant-bisphenol A, methylene blue and neutral red onto a novel bagasse-β-cyclodextrin polymer by adsorption process. Chemosphere 259:127439. https://doi.org/10.1016/j.chemosphere.2020.127439

Naidu R, Arias Espana VA, Liu Y, Jit J (2016) Emerging contaminants in the environment: Risk-based analysis for better management. Chemosphere 154:350–357. https://doi.org/10.1016/j.chemosphere.2016.03.068

Ndagijimana P, Liu X, Li Z et al (2019) Optimized synthesis of a core-shell structure activated carbon and its adsorption performance for Bisphenol A. Sci Total Environ 689:457–468. https://doi.org/10.1016/j.scitotenv.2019.06.235

Nogueira M, Matos I, Bernardo M, et al (2019) Char from spent tire rubber: a potential adsorbent of remazol yellow dye. C 5:76. https://doi.org/10.3390/c5040076

Noori M, Tahmasebpoor M, Foroutan R (2022) Enhanced adsorption capacity of low-cost magnetic clinoptilolite powders/beads for the effective removal of methylene blue: Adsorption and desorption studies. Mater Chem Phys 278:125655. https://doi.org/10.1016/j.matchemphys.2021.125655

Ong LK, Soetaredjo FE, Kurniawan A et al (2014) Investigation on the montmorillonite adsorption of biocidal compounds incorporating thermodynamical-based multicomponent adsorption isotherm. Chem Eng J 241:9–18. https://doi.org/10.1016/j.cej.2013.12.001

Patawat C, Silakate K, Chuan-Udom S et al (2020) Preparation of activated carbon from *Dipterocarpus alatus* fruit and its application

for methylene blue adsorption. RSC Adv 10:21082–21091. https://doi.org/10.1039/D0RA03427D
Pezoti O, Cazetta AL, Souza IPAF et al (2014) Adsorption studies of methylene blue onto ZnCl2-activated carbon produced from buriti shells (Mauritia flexuosa L.). J Ind Eng Chem 20:4401–4407. https://doi.org/10.1016/j.jiec.2014.02.007
Ramaraju B, Manoj Kumar Reddy P, Subrahmanyam C (2014) Low cost adsorbents from agricultural waste for removal of dyes. Environ Prog Sustain Energy 33:38–46. https://doi.org/10.1002/ep.11742
Ratkowsky D, Giles D (1990) Handbook of nonlinear regression models | Wageningen University and Research Library catalog. https://library.wur.nl/WebQuery/titel/344991. Accessed 24 Jun 2024
Rout PR, Bhunia P, Dash RR (2014) Modeling isotherms, kinetics and understanding the mechanism of phosphate adsorption onto a solid waste: Ground burnt patties. J Environ Chem Eng 2:1331–1342. https://doi.org/10.1016/j.jece.2014.04.017
Saleh TA, Sarı A, Tuzen M (2017) Optimization of parameters with experimental design for the adsorption of mercury using polyethylenimine modified-activated carbon. J Environ Chem Eng 5:1079–1088. https://doi.org/10.1016/j.jece.2017.01.032
San Miguel G, Lambert SD, Graham NJD (2001) The regeneration of field-spent granular-activated carbons. Water Res 35:2740–2748. https://doi.org/10.1016/S0043-1354(00)00549-2
Shahrokhi-Shahraki R, Benally C, El-Din MG, Park J (2021) High efficiency removal of heavy metals using tire-derived activated carbon vs commercial activated carbon: Insights into the adsorption mechanisms. Chemosphere 264:128455. https://doi.org/10.1016/j.chemosphere.2020.128455
Shao P, Pei J, Tang H et al (2021) Defect-rich porous carbon with anti-interference capability for adsorption of bisphenol A via long-range hydrophobic interaction synergized with short-range dispersion force. J Hazard Mater 403:123705. https://doi.org/10.1016/j.jhazmat.2020.123705
Sirimuangjinda A, Hemra K, Atong D, Pechyen C (2013) Comparison on pore development of activated carbon produced from scrap tire by potassium hydroxide and sodium hydroxide for active packaging materials. Key Eng Mater 545:129–133. https://doi.org/10.4028/www.scientific.net/KEM.545.129
Sokolov S, Zyrina A, Akimov S et al (2023) Toxic effects of penetrating cations. Membranes 13:841. https://doi.org/10.3390/membranes13100841
Soliman NK, Moustafa AF (2020) Industrial solid waste for heavy metals adsorption features and challenges; a review. J Mater Res Technol 9:10235–10253. https://doi.org/10.1016/j.jmrt.2020.07.045
Sudhakar P, Mall ID, Srivastava VC (2016) Adsorptive removal of bisphenol-A by rice husk ash and granular activated carbon—a comparative study. Desalination Water Treat 57:12375–12384. https://doi.org/10.1080/19443994.2015.1050700
Sun Z, Zhao L, Liu C et al (2020) Fast adsorption of BPA with high capacity based on π-π electron donor-acceptor and hydrophobicity mechanism using an in-situ sp2 C dominant N-doped carbon. Chem Eng J 381:122510. https://doi.org/10.1016/j.cej.2019.122510
Tabatabaei SM, Dastmalchi S, Mehrizad A, Gharbani P (2011) Enhancement of 4-nitrophenol ozonation in water by nano ZnO catalyst. Iranian J Environ Health Sci Eng 8:363
Tang D, Zhang G (2016) Efficient removal of fluoride by hierarchical Ce–Fe bimetal oxides adsorbent: Thermodynamics, kinetics and mechanism. Chem Eng J 283:721–729. https://doi.org/10.1016/j.cej.2015.08.019
Tokula BE, Dada AO, Inyinbor AA et al (2023) Agro-waste based adsorbents as sustainable materials for effective adsorption of Bisphenol A from the environment: a review. J Clean Prod 388:135819. https://doi.org/10.1016/j.jclepro.2022.135819
Tran HN, You S-J, Chao H-P (2017) Fast and efficient adsorption of methylene green 5 on activated carbon prepared from new chemical activation method. J Environ Manage 188:322–336. https://doi.org/10.1016/j.jenvman.2016.12.003
Tursi A, Chatzisymeon E, Chidichimo F et al (2018) Removal of endocrine disrupting chemicals from water: adsorption of bisphenol-A by biobased hydrophobic functionalized cellulose. Int J Environ Res Public Health 15:2419. https://doi.org/10.3390/ijerph15112419
Üzek R, Şenel S, Denizli A (2022) Investigation of thermodynamic, kinetic, and isothermal parameters for the selective adsorption of bisphenol A. ACS Omega 7:18940–18952. https://doi.org/10.1021/acsomega.2c01975
Vandenberg LN, Hauser R, Marcus M et al (2007) Human exposure to bisphenol A (BPA). Reprod Toxicol 24:139–177. https://doi.org/10.1016/j.reprotox.2007.07.010
Wang J, Guo X (2022) Rethinking of the intraparticle diffusion adsorption kinetics model: interpretation, solving methods and applications. Chemosphere 309:136732. https://doi.org/10.1016/j.chemosphere.2022.136732
Wang S, Zhu ZH, Coomes A et al (2005) The physical and surface chemical characteristics of activated carbons and the adsorption of methylene blue from wastewater. J Colloid Interface Sci 284:440–446. https://doi.org/10.1016/j.jcis.2004.10.050
Wang ZB, Tian YJ, Wang XK (2014) Adsorption performance to methylene blue by non-activated tire-based pyrolytic char. Appl Mech Mater 508:35–39. https://doi.org/10.4028/www.scientific.net/AMM.508.35
Weber WJ, Morris JC (1963) Closure to "kinetics of adsorption on carbon from solution." J Sanit Eng Div 89:53–55. https://doi.org/10.1061/JSEDAI.0000467
Xie X, Ma X, Guo L et al (2019) Novel magnetic multi-templates molecularly imprinted polymer for selective and rapid removal and detection of alkylphenols in water. Chem Eng J 357:56–65. https://doi.org/10.1016/j.cej.2018.09.080
Xue H, Wang X, Xu Q et al (2021) Adsorption of methylene blue from aqueous solution on activated carbons and composite prepared from an agricultural waste biomass_ A comparative study by experimental and advanced modeling analysis. Chem Eng J 430:132801
Yuh-Shan H (2004) Citation review of Lagergren kinetic rate equation on adsorption reactions. Scientometrics 59:171–177. https://doi.org/10.1023/B:SCIE.0000013305.99473.cf
Zerin NH, Rasul MG, Jahirul MI, Sayem ASM (2023) End-of-life tyre conversion to energy: a review on pyrolysis and activated carbon production processes and their challenges. Sci Total Environ 905:166981. https://doi.org/10.1016/j.scitotenv.2023.166981
Zhang J, Gao J, Chen Y et al (2017) Characterization, preparation, and reaction mechanism of hemp stem based activated carbon. Results Phys 7:1628–1633. https://doi.org/10.1016/j.rinp.2017.04.028
Zhuang S, Chen R, Liu Y, Wang J (2020) Magnetic COFs for the adsorptive removal of diclofenac and sulfamethazine from aqueous solution: adsorption kinetics, isotherms study and DFT calculation. J Hazard Mater 385:121596. https://doi.org/10.1016/j.jhazmat.2019.121596